Molecular motion and phase transition in K_3C_{60} and Rb_3C_{60} by nuclear magnetic resonance

Y. Yoshinari,* H. Alloul, V. Brouet, G. Kriza,† and K. Holczer‡
Laboratoire de Physique des Solides, URA2 CNRS, Université Paris-Sud, 91405 Orsay, France

L. Forro
Laboratoire de Physique des Solides Semicristallins, Département de Physique, Ecole Polytechnique Fédérale de Lausanne, 1015-Lausanne, Switzerland

(Received 17 April 1996)

Nuclear magnetic resonance (NMR) has been performed to study the molecular dynamics of the C_{60} molecule in K_3C_{60} and Rb_3C_{60}. It is shown that the hypothesis of a uniaxial rotational motion around an axis fixed in the crystal can satisfactorily explain the observed ^{13}C NMR results. A resonance line is detected in the ^{39}K and ^{87}Rb NMR spectra below a temperature T^* of 200 and 380 K in K_3C_{60} and Rb_3C_{60}, respectively. In particular, this T^* in K_3C_{60} coincides with the temperature at which we observed a phase transition. This provides some clue about the origin of the phase transition. The discrepancy between the observed and calculated ^{13}C line shapes at low temperature suggests that the freezing of the molecular motion and a structural change at the phase transition induce a significant modification of the electron density on the C_{60} molecule and likely on the conduction band electronic state. [S0163-1829(96)06734-3]

I. INTRODUCTION

Since the discovery of buckminsterfullerene (C_{60}),[1] a variety of research subjects on this icosahedral molecule have been developed in chemistry and solid state physics. Successful synthesis of superconducting alkali doped compositions [M_3C_{60} (M=K and Rb)] with the relatively high transition temperature T_c (about 30 K for Rb_3C_{60}) has opened another research area. The interest in solid state physics is not limited to superconductivity and metallic properties.[2,3] Because of its highly symmetrical molecular shape, the C_{60} molecule has quite unique molecular motions in crystals. In the pristine C_{60} compound, a random reorientation of the C_{60}, with time scale of the order of 10^{-11} sec, has been proposed to occur at room temperature.[4–6] Below an orientationally disordered-ordered phase transition temperature around 250 K, an anisotropic uniaxial rotation takes place.[7,8] Its axes appear to be preferentially established along four equivalent $\langle 1,1,1\rangle$ directions. The existence of the similar uniaxial motion has been confirmed even in K_3C_{60} by Yoshinari *et al.* from ^{13}C-NMR measurements.[9] A similar NMR analysis in insulating K_4C_{60} has also been made by Zimmer *et al.*[10] The existence of the uniaxial motion in alkali doped compounds enlightens an essential role of the alkali ions in the series of M_3C_{60}, which not only transfer charges onto the C_{60}, but also change the crystal field at the C_{60}. The occurrence of the anisotropic motion implies that the symmetry on the C_{60} molecule is lower than cubic. Such distortion of the crystal field might lift the degeneracy of the conduction band which originates from the triply degenerate lowest unoccupied molecular orbital (LUMO) of the C_{60} molecule, and affect the electronic properties.

We should like to note that the C_{60} molecules in the crystal are well separated (the nearest-neighbor distance is approximately 10 Å while the diameter of the C_{60} molecule is 7.1 Å).[11] Thus the narrow band associated with the small overlap of carbon $2p_\pi$ orbitals is responsible for the metallic properties. The degree of overlap is sensitively affected by the relative position of carbons of different C_{60}. Therefore, the low temperature (T) electronic properties of the materials are certainly determined by the actual structure after freezing of the molecular motion. Furthermore, in the M_3C_{60} compounds, a merohedral disordered fcc structure has been proposed from the analysis of low temperature x-ray data, where the C_{60} molecule occupies randomly one of two orientations which can be deduced from each other by a 90° rotation with respect to the cubic sides.[11,12] This results in three distinct carbon sites relative to the alkali ions, for which the electronic density possibly varies.

Related to the above issue concerning the crystal structure in low T, it should be noted that a phase transition at 200 K has been found in K_3C_{60},[9] although no evidence for a structural change has been found yet by x-ray experiments. An identification of the molecular motion and a clarification of the connection between the phase transition and the freezing of the molecular motion are quite important to understand the low T electronic state.

In this paper, we shall mainly address the dynamics of the molecular motion and the phase transition. A numerical analysis based on the ^{13}C-NMR results will be presented to clarify the nature of the molecular motion. The agreement between the calculated and observed line shapes, together with an interpretation of drastic changes in the spectra, allow us to evidence the existence of the uniaxial anisotropic motion of the C_{60} molecule in K_3C_{60} and Rb_3C_{60}. Although a similar line shape analysis has also been done by Blinc *et al.* for the pristine C_{60} compound,[13] our model has been extended to interpret the spin-lattice relaxation rate, T_1^{-1}, and gives numerical estimates quite consistent with the data taken in K_3C_{60}. We also report NMR experimental results performed for the alkali nuclei ^{39}K and ^{87}Rb in the two compounds. Appearance of an extra peak in the ^{39}K spectrum around the phase transition temperature, whose behavior is quite identical to that previously reported for the ^{87}Rb spec-

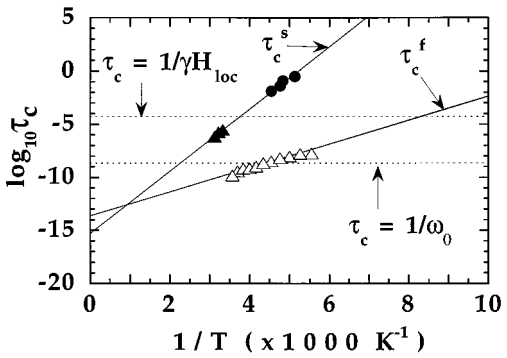

FIG. 1. Temperature dependence of the correlation times τ_c. The open and solid triangles are the τ_c extracted from the observed T_1, and T_2, respectively. The solid circles are the one reported by Barret and Tycko (Ref. 15). Solid lines are the results fitted to an Arrenius law (Ref. 9), for τ_c^s and τ_c^f.

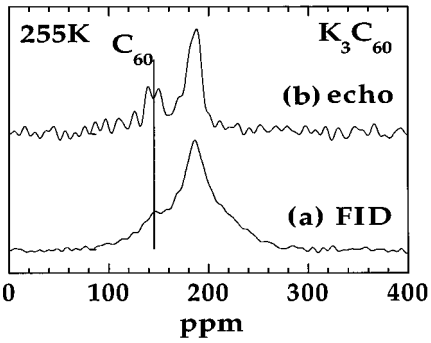

FIG. 2. Fourier transform spectra of the ^{13}C FID (a) and spin-echo (b) signals, measured at 255 K in K_3C_{60}. The vertical line around 140 ppm indicates the location of the pure C_{60} signal contained in our K_3C_{60} sample.

trum below 380 K,[14] provides some clue to understand the low temperature phase.

This paper is organized as follows. The NMR results for the ^{13}C nucleus as well as those for ^{39}K and ^{87}Rb nuclei in K_3C_{60} and Rb_3C_{60} will be shown in the next section and will allow one to grasp the similarities and differences between the two compounds. The formalism used to describe the NMR shift tensor at a carbon site and the T_1^{-1} in the presence of the uniaxial rotation will be given in Sec. III. The NMR line shape calculated for an axial and a nonaxial symmetry of the shift anisotropy, and the recovery curve of the nuclear magnetization which allow to determine T_1 will be demonstrated in Sec. IV together with the comparison with the data. The origin of the phase transition and the appearance of the extra peak in the cation NMR spectra will be briefly discussed in Sec. V in connection with the molecular motion.

II. EXPERIMENTAL RESULTS

A. K_3C_{60}

1. ^{13}C NMR

In our previous paper,[9] we reported the existence of two distinct correlation times (τ_c) related to the molecular motions of the C_{60} in K_3C_{60}. The T dependence of the fast τ_c^f was extracted from an observed broad peak in T_1^{-1}, while that of the slow τ_c^s was deduced from a combination of data on the spin-spin relaxation rate T_2^{-1} around 300 K and from that reported by Barret and Tycko.[15] Figure 1 summarizes our main results about the correlation times. The slopes of each τ_c allowed to determine the activation parameters for the corresponding motions by fitting to an Arrenius law. The respective activation energies for the fast (τ_c^f) and slow (τ_c^s) motions were estimated to be 2600 and 6800 K. It is noted that the former value is similar to the one determined by NMR (Refs. 4 and 6) in pristine C_{60} in the low T phase below the transition temperature.

The existence of two τ_c's raised an important question about an eventual inhomogeneity of the molecular motion. Do these motions take place on the same C_{60} molecule or do they occur on different molecules? The answer was given by comparing Fourier transform (FT) spectra obtained from a free induction decay signal (FID) and a spin-echo signal. While the FID signal includes all signals whatever τ_c, the spin echo signal selects a window of τ_c values. Since the decay function of the spin-echo signal roughly obeys to $\exp(-At\tau_c)$, a signal component corresponding to the slow (large) τ_c is expected to vanish at a sufficiently long t, which is seen as a disappearance of the corresponding structure in the FT spectrum taken from the spin echo signal.

Figure 2 demonstrates the FT spectra obtained from the FID signal (a) and from the spin-echo signal (b) at 255 K. The difference in the spectra is obvious, the broad tail observed in the FID spectrum disappears in the echo spectrum. This fact led us to assign the tail to the slow τ_c^s. However, the measurement of the T_1 at the tail gave rise to the same temperature dependence and magnitude of T_1 as those measured at the peak.[9] Since the two τ_c values are so different in the investigated T range the T_1 would be significantly different in order of magnitude, if the two τ_c values characterized motions occurring on distinct molecules. These observations mentioned above therefore allowed us to conclude that the ^{13}C atoms which give rise to the tail part of the spectrum are involved in the two molecular motions. This fact also means that the two motions with markedly different time scales take place on the same molecules, and that the molecular motions are homogeneous throughout the material.

Another important observation in our previous paper was an occurrence of a phase transition around 200 K evidenced by a clear anomaly in the differential thermal analysis (DTA) measurements and an abrupt increase of the linewidth of the FID spectrum, as shown in Fig. 3. The fact that the shape of the DTA signal at 200 K was the same as that due to the C_{60} contamination in our sample observed at 260 K supports the occurrence of a phase transition. Although the two anomalies (Fig. 3) observed in the linewidth around 90 and 270 K can be attributed to the slowing down of the activated motions in Fig. 1, which occur for $\gamma H_0 \tau_c \approx 1$, the anomaly at 200 K cannot be interpreted by these activation processes.

It is also very important to clarify whether or not the molecular motion persists below the phase transition. Figure 4 shows a comparison of two spectra measured at 255 K (solid line) and 160 K (dotted line) with different horizontal scales. Although a larger anisotropy of the shift is required to explain the spectrum at 160 K, the two spectra are very similar to each other. As demonstrated in Sec. IV, this character-

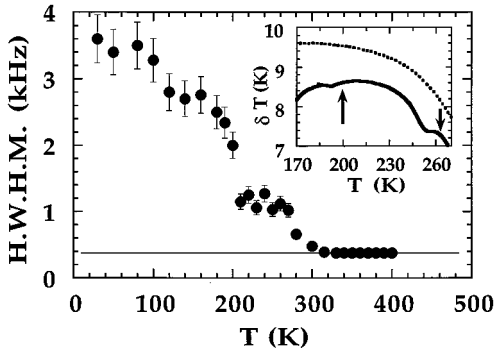

FIG. 3. Main: Temperature dependence of the half width at half maximum of the ^{13}C peak in K_3C_{60}. Inset: The solid and dotted lines are DTA signals of K_3C_{60} and of the background. The arrows indicate the onsets of the phase transitions.

istic line shape can be nicely reproduced by the uniaxial motion model. It can therefore be concluded that the phase transition is not accompanied with a total freezing of the motion. From this point of view, it is unlikely to assign the abrupt change in linewidth at 200 K to a freezing of the molecular motion. The increase of the linewidth should rather be attributed to a modification of the electronic state on the C_{60} caused by the phase transition.

2. ^{39}K NMR

We have performed ^{39}K-NMR measurements on the sample used for the ^{13}C NMR,[16] to study the influence of the slowing down of the rotational motion and of the phase transition on the alkali sites. Figure 5 shows the ^{39}K FT spectra taken from the FID signal. The two lines observed at 300 K exhibit a relative intensity ratio of 1:2 (within the experimental error of 2%). From the known room T crystal structure,[11] these lines are immediately assigned to the octahedral (O:1) and tetrahedral (T:2) sites. Let us point out here that within the accuracy of the data we can conclude that the stoichiometry is not far from 2.

As can be seen in Fig. 5, an additional small line T' shows up around 200 K. The relative intensity determined at 200 K was 36:54:10 (within error ± 4) for the O, T, and T', respectively. Let us indicate here that this line is quite similar

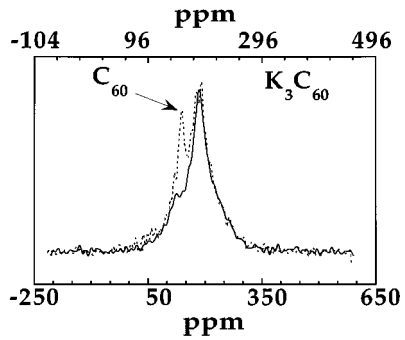

FIG. 4. Fourier transform spectra of ^{13}C FID signals in K_3C_{60} measured at 255 K (solid line) and 160 K (dotted line). The horizontal axes have been scaled to bring the spectra into coincidence (lower scale is for 160 K, and upper scale for 255 K).

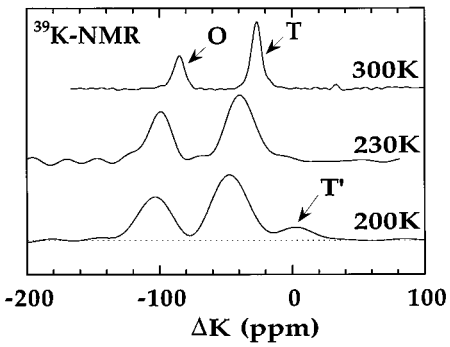

FIG. 5. Fourier transformed spectra of ^{39}K FID signals in K_3C_{60} measured at the temperature indicated. The T, O, and T' stand for the tetrahedral, octahedral, and new peak assigned to the T site offset from the ideal position, respectively (details in text). The reference frequency is taken as the resonance of KCl.

to that observed in Rb_3C_{60} by Walstedt *et al.*, which disappears above 400 K.[14] The appearance of this extra peak implies that a new K site with different electronic state is established around 200 K, at which the phase transition is detected. Note that the T' line has a similar linewidth to that of the T or O lines at the same temperature. This means that the shift of the T' line is mainly due to a difference in magnetic hyperfine coupling, and not to a quadrupolar effect.[18]

The slowing down of the rotational motion of the C_{60} molecule and the occurrence of the phase transition are also monitored through the T dependence of the linewidth of the ^{39}K lines. This is shown in Fig. 6. The linewidths at the two ^{39}K sites increase rapidly around 240 K, and displays a change in its T dependence at 200 K. The fact that the broadening occurs at the two sites nearly in the same way, implies that the two sites probe the same phenomenon. If we consider that the anisotropy of the local field at the cation sites is at most 25 ppm (estimated from the linewidth at 4.2 K) which corresponds to 300 Hz at the operating resonance frequency of 14.88 MHz, the extrapolation of the τ_c in Fig. 1 to low temperature allows to expect that the slowing down of the motions should induce a broadening of the ^{39}K line at about 240 and 96 K for the perpendicular and fast uniaxial rotational motions, respectively. The fact that the observed broadening sets in around 240 K is therefore due to the slowing down of the perpendicular motion. The change of the

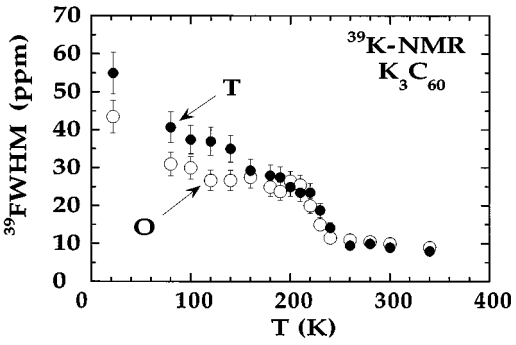

FIG. 6. Temperature dependence of the full width at half maximum of the ^{39}K peaks in K_3C_{60}. The solid and open circles are the ones for tetrahedral(T) and octahedral(O) K sites, respectively.

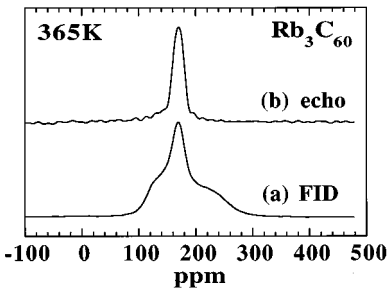

FIG. 7. Fourier transformed spectra of ^{13}C FID signals (a) and spin echo (b) measured at 365 K in Rb_3C_{60}.

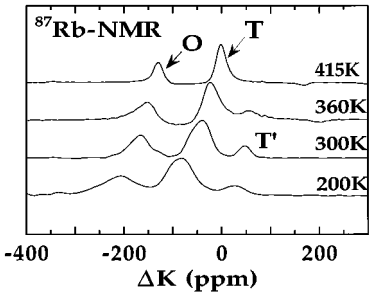

FIG. 8. Fourier transformed spectra of ^{87}Rb FID signals in Rb_3C_{60} measured at the temperatures indicated. The T, O, and T' stand for the tetrahedral, octahedral, and new line assigned to the T site slightly offset from the ideal position, respectively (details in text). The reference frequency is taken at the NMR frequency of RbCl.

broadening rate at 200 K provide additional evidence that the dynamics in the system is suddenly modified by the phase transition. This is consistent with the abrupt change in ^{13}C linewidth at 200 K (Fig. 3). So all the anomalies observed at 200 K suggest a strong connection between the phase transition, the appearance of the third line in the potassium NMR and the freezing of the perpendicular motion.

B. Rb_3C_{60}

The fact that a third line T' has been seen in the ^{87}Rb spectra below 400 K indicates that some similarity exists between the two systems. It is then quite interesting to compare the molecular motions and the phase transition on the two systems. Previous work by Tycko *et al.* reported ^{13}C spectra below room T, presumably associated with a slowing down of some molecular motion at low T.[17] More accurate studies of the ^{13}C spectral shapes are required, in order to understand the relationship of the molecular motions with the appearance of the T' line.

1. ^{13}C NMR

The ^{13}C line is still narrow at a temperature where the T' line appears [in Fig. 7, ^{13}C-NMR spectra taken at $T=365$ K, from the FID (a) and from the spin echo (b) are displayed]. As has been shown for K_3C_{60}, the fast uniaxial molecular motion persists below the temperature at which the T' line appears. Although the FID spectrum exhibits a line shape different from that found in K_3C_{60}, the disappearance of the tail in the spin-echo spectrum strongly suggests the existence of the uniaxial molecular motion similar to that in K_3C_{60}. The observed line shape can also be well reproduced in terms of the uniaxial motion as will be demonstrated in Sec. IV.

2. ^{87}Rb NMR

Figure 8 demonstrates the T dependence of ^{87}Rb FT spectra obtained from FID signal on Rb_3C_{60}. Two lines observed at 420 K have a relative intensity ratio of 1:2 (within the error of 4%), as expected from the crystal structure. It should be pointed out that the third peak has also been found in Rb_3C_{60} around 370 K. The relative intensity determined at 300 K was 34:54:11 (with error of ± 2) for the O, T, and T', respectively. This intensity ratio is quite similar to that in K_3C_{60}. This fact might also imply the phase transition temperature in Rb_3C_{60} around 370 K, which is twice as high as that in K_3C_{60}. We will discuss the possible origin of this extra peak in connection with the phase transition in Sec. V.

III. BASIC FORMULATION

We describe here the model used to calculate the ^{13}C NMR spectra and magnetization recovery. We assume that in the fast motion (τ_c^f) the C_{60} molecule rotates back and forth around an axis fixed in the lattice frame. The slow motion (τ_c^s) is an occasional flip of the C_{60} molecule around axes perpendicular to the fast rotation axis which is kept unchanged. The time scale τ_c^s is assumed to satisfy $(\gamma H_{\rm loc})^{-1} < \tau_c^s < T_1$. The former inequality implies that the uniaxial motion is well established so that the spectrum is characteristic of the fast motion, while the consequence of the latter is that the eventual distribution of T_1 values for the various ^{13}C on the C_{60} molecule, is averaged by the perpendicular motion. To represent the experimental situation, for which powder samples are used, we consider a single C_{60} molecule and take into account all possible directions of the rotation axis with respect to the applied magnetic field. In order to simplify the calculations, the icosaedral symmetry of the molecule is neglected, and the density of carbon atoms is assumed to be uniformly distributed on the C_{60} molecule. This assumption would eventually not be valid for experiments in single crystals, for which the spectra could, for some orientations of the applied field, depend on the relative orientations of the symmetry axis of the molecule with respect to the crystalline axes.

A. NMR spectra

We will start with the derivation of a formula which describes the NMR shift at a given carbon atom in the laboratory frame in the presence of the uniaxial motion. We define the shift tensor of the carbon site in an atomic reference frame as (K_x, K_y, K_z). The shift component K_z is normal to the sphere, while K_x, K_y are those in the tangential plane to the sphere. The principal directions of the in-plane shifts on each carbon site are fixed in the atomic frame, but their directions are unknown at each carbon site. Therefore, we shall take them as arbitrary. The in-plane shift components of the K_x and K_y should be replaced by $(K_x\cos^2\phi + K_y\sin^2\phi)$ and $(K_x\sin^2\phi + K_y\cos^2\phi)$, where ϕ is uniformly distributed. To simplify the written formulas we hereafter represent this shift tensor as (K_1, K_2, K_3).

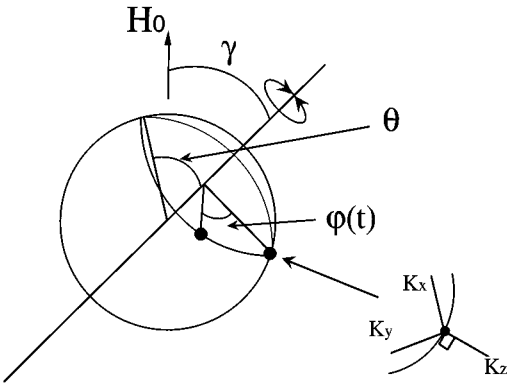

FIG. 9. Definition of the angles γ, $\varphi(t)$, and θ.

In order to specify the position of the carbon site during the motion, we need three independent angles specified in Fig. 9. The first one (γ) specifies the position of the rotation axis with respect to the external magnetic field applied along the Z direction in the laboratory frame. The second is the longitude (θ) of the atom with respect to the rotation axis, which does not vary during the fast motion. The third angle $\varphi(t)$ involves the time dependence, and allows to describe the random jump of the atom on its circular locus in the fast motion. The shift tensor in the laboratory frame is obtained by applying three Euler matrices to the shift tensor in the atomic frame, each of which represents the angular operations mentioned above. The final result which describes the actual NMR shift along the Z direction is

$$\begin{aligned}\sigma_{ZZ}(t)=&\{D_{11}\cos^2\varphi(t)+D_{22}\sin^2\varphi(t)\\&-\tfrac{1}{2}\,(D_{12}+D_{21})\sin2\varphi(t)\}\sin^2\gamma\\&-\tfrac{1}{2}\,\{(D_{13}+D_{31})\cos\varphi(t)-(D_{23}+D_{32})\\&\times\sin\varphi(t)\}\sin2\gamma+D_{33}\cos^2\gamma. \qquad (1)\end{aligned}$$

where

$$D_{11}=K_1\cos^2\theta+K_3\sin^2\theta,$$

$$D_{22}=K_2,$$

$$D_{33}=K_1\sin^2\theta+K_3\cos^2\theta,$$

$$D_{12}=D_{21}=\tfrac{1}{2}(K_x-K_y)\sin2\phi\cos\theta,$$

$$D_{13}=D_{31}=\tfrac{1}{2}(K_1-K_3)\sin2\theta,$$

$$D_{23}=D_{32}=\tfrac{1}{2}(K_x-K_y)\sin2\phi\,\sin\theta. \qquad (2)$$

The σ_{XX}, σ_{YY}, and other off-diagonal elements can also be calculated in the same way.

If the rotation motion is very fast, we can replace the square and the linear terms of $\sin\varphi(t)$ and $\cos\varphi(t)$ by 1/2 and 0, respectively. Then, Eq. (1) becomes

$$\begin{aligned}\sigma_{ZZ}=&\tfrac{1}{2}(K_1\cos^2\theta+K_2+K_3\sin^2\theta)\sin^2\gamma\\&+(K_1\sin^2\theta+K_3\cos^2\theta)\cos^2\gamma. \qquad (3)\end{aligned}$$

Characteristic of the uniaxial rotation motion is that, contrary to the case of an isotropic rotational motion, all the carbons on the C_{60} molecule no longer exhibit a unique value of the shift. As seen in Eqs. (1) and (3), the averaged shift depends both on θ and γ.

It should be noted that Eq. (3) can also be rewritten as

$$\begin{aligned}\sigma_{ZZ}=&(K_1+K_2+K_3)\cos^2\gamma+\tfrac{1}{2}(1-3\cos^2\gamma)\\&\times(K_1\cos^2\theta+K_2+K_3\sin^2\theta). \qquad (4)\end{aligned}$$

This expression allows to display that σ_{ZZ} becomes independent of θ for the so-called magic angle $\gamma\sim54.7°$, obtained for $(1-3\cos^2\gamma)=0$. We find that the line shape for the C_{60} rotating at the magic angle is a δ function at $K_{\rm iso}=(K_1+K_2+K_3)/3$, as expected from the general result at the basis of magic angle spinning NMR experiments in solids.[19]

In the line shape calculation, since the in-plane shift anisotropy on the carbon site is unknown, we summed up all line shapes originating from different ϕ with equal probability, except for $K_x=K_y$. To reproduce the actual spectra we must also take into account the distribution of γ, which is given by the derivative element $\sin\gamma\,d\gamma$. The different number of carbon sites at a given θ contributes to the line shape with a weight $\sin\theta\,d\theta$ in the uniform density approximation done here.

B. Spin lattice relaxation rate T_1^{-1}

We shall now proceed a calculation of the spin lattice relaxation rate T_1^{-1} in the presence of the uniaxial motion of the C_{60} molecule, and use the formalism given in Refs. 19 and 20. T_1^{-1} is defined as the coefficient of the recovery of the longitudinal component of the spin operator,

$$\frac{d}{dt}\langle I_z\rangle=-\frac{1}{T_1}\,(\langle I_z\rangle-\langle I_z\rangle_0). \qquad (5)$$

The expectation value of the spin $\langle I_z\rangle$ is given by use of a density matrix ρ via $\langle I_z\rangle=\mathrm{Tr}\{\rho(t)I_z\}$. Once the Hamiltonian in the laboratory frame is given in the form $H^L(t)=\Sigma_{j,m,n}F^L_j(t)A^L_m(n)\exp(im\omega_0 t)$, the time evolution of $\rho(t)$ is described by[19]

$$\frac{d}{dt}\,\rho(t)=-\frac{1}{2}\sum_{j,m,n}\mathcal{I}_j(m\omega_0)[A^L_m(-n),[A^L_m(n),\rho(t)-\rho_0]], \qquad (6)$$

where

$$\mathcal{I}_j(m\omega_0)=\int_{-\infty}^{\infty}\Phi_{j,j}\exp(-im\omega_0 t)\,dt,$$

$$\Phi_{j,j}(\tau)=\langle F_j(t)F_j(t+\tau)\rangle. \qquad (7)$$

$\langle\,\rangle$ is an ensemble average. Here, we made use of the fact that nonsecular products in A and F in Eqs. (6) and (7) are zero. The characteristic contributions of the motion to T_1^{-1} appear through the correlation function F defined in the second equation of Eq. (7).

A shift Hamiltonian $\mathbf{I}\cdot\sigma\cdot\mathbf{H}$ in an atomic frame of reference can be expressed by

$$H^M=\sum_q F_q^M A^M(q), \qquad \begin{matrix} F_0^M=\dfrac{\gamma\delta}{2}, \\ F_{\pm 1}^M=0, \\ F_{\pm 2}^M=\gamma\delta\eta, \end{matrix} \qquad \begin{matrix} A^M(0)=3H_zI_z-\mathbf{H}\cdot\mathbf{I}, \\ A^M(\pm 1)=0, \\ A^M(\pm 2)=\frac{1}{4}(H^+I^++H^-I^-), \end{matrix} \tag{8}$$

where the anisotropic part of the shift tensor δ and its asymmetry parameter η are defined in

$$K_x=K_{\rm iso}-\frac{\delta}{2}(1+\eta), \quad K_y=K_{\rm iso}-\frac{\delta}{2}(1-\eta),$$

$$K_z=K_{\rm iso}+\delta. \tag{9}$$

The time modification of the shift Hamiltonian induced by the molecular motions becomes a source for the T_1^{-1}. The time dependence of the Hamiltonian in the laboratory frame can be obtained by transforming that in the atomic frame through a unitary matrix, $\mathbf{U}(\Omega)$, which describes the motion, that is, $\mathbf{I}\cdot\mathbf{U}^{-1}\sigma\mathbf{U}\cdot\mathbf{H}$, where the $\mathbf{I}$ and $\mathbf{H}$ are redefined as the spin operator and the external field in the laboratory frame. Then the Hamiltonian can be written

$$H^L(t)=\sum_{\substack{n,j=0,\pm 1,\pm 2 \\ k=\rm Re,Im}} F_j^L C_{k\,j,n}(\Omega(t))\alpha_k(j,n)A_k^L(n) \times\exp(-i\omega_0 t), \tag{10}$$

$$F_0^L=\frac{\gamma\delta}{2}, \quad F_{\pm 1}^L=0, \quad F_{\pm 2}^L=\frac{\gamma\delta\eta}{2\sqrt{6}}, \tag{11}$$

$$A_{\rm Re}^L(0)=3H_ZI_Z-\mathbf{H}\cdot\mathbf{I} \quad A_{\rm Im}^L(0)=0,$$

$$A_{\rm Re}^L(\pm 1)=\tfrac{1}{2}\{H_Z(I^++I^-)+(H^++H^-)I_Z\},$$

$$A_{\rm Im}^L(\pm 1)=\frac{1}{i2}\{H_Z(I^+-I^-)+(H^+-H^-)I_Z\},$$

$$A_{\rm Re}^L(\pm 2)=\tfrac{1}{4}(H^+I^++H^-I^-),$$

$$A_{\rm Im}^L(\pm 2)=\frac{1}{i4}(H^+I^+-H^-I^-). \tag{12}$$

The imaginary terms in the A's appear in the process of the transformation. The C's contain the motion parameters, while the α's arise from the fact that the unitary matrix is normalized. As a simple example for which the moving atom can be specified by two Euler angles defined in an ordinary polar coordinate, the $C_{k,j,n}(\Omega(t))$ and $\alpha_k(j,n)$ are given in Appendix A.

When two distinct motions, that is, a uniaxial rotation motion plus perpendicular flips take place, the correlation function is written by[20]

$$\begin{aligned}\Phi_{j,j}(\tau)=\frac{1}{5}(F_j^L)^2[&C_{j,-2}C_{j,+2}\exp\{-(4E_{\rm rot}+2E_{\rm flip})\tau\} \\ &+C_{j,+2}C_{j,-2}\exp\{-(4E_{\rm rot}+2E_{\rm flip})\tau\} \\ &+C_{j,-1}C_{j,+1}\exp\{-(E_{\rm rot}+5E_{\rm flip})\tau\} \\ &+C_{j,+1}C_{j,-1}\exp\{-(E_{\rm rot}+5E_{\rm flip})\tau\} \\ &+C_{j,0}C_{j,0}\exp\{-6E_{\rm flip}\tau\}].\end{aligned} \tag{13}$$

Here $E_{\rm rot}$ and $E_{\rm flip}$ are rotational diffusion constants for the fast rotation motion and the perpendicular flip, respectively. The C's will be given later. Since in our case the correlation time (diffusion constant) of the perpendicular flip is more than six orders of magnitude slower (smaller) than the one of the uniaxial rotation motion in the T range investigated, we could safely put $E_{\rm flip}=0$. Therefore the last term in Eq. (13) does not contribute to the relaxation of the nuclear spin. This assumption allows to simplify Eq. (13) into

$$\begin{aligned}\Phi_{j,j}(\tau)\approx\frac{2}{5}(F_j^L)^2[&|C_{j,+2}|^2\exp(-4E_{\rm rot}\tau) \\ &+|C_{j,+1}|^2\exp(-E_{\rm rot}\tau)].\end{aligned} \tag{14}$$

However, this does not mean that the slow motion does not play any role. Indeed, while the rotational diffusion constant of the perpendicular flip does not affect the T dependence of T_1^{-1}, this motion still plays a role as it effectively averages the θ dependence of T_1^{-1} as long as it occurs on a time scale faster than the observed T_1. This argument allows us to average the $|C|^2$ over the ϕ, θ, and $\varphi(t)$ without any weight function, and thus T_1^{-1} depends only on γ, which is the angle between the external field and the rotating axis of the C_{60}.

Another issue is the evaluation of T_1^{-1} from the shift components known from the static NMR parameters. The deduced value for T_1^{-1} depends on the way in which the three independent shift tensor parameters are assigned to the different spatial orientations. Within our assumptions, three cases are naturally distinguished depending upon which shift component is associated with z:

$$\text{(case 1)} \quad K_x=K_{\rm iso}-\frac{\delta}{2}(1+\eta), \quad K_y=K_{\rm iso}-\frac{\delta}{2}(1-\eta),$$

$$K_z=K_{\rm iso}+\delta,$$

$$\text{(case 2)} \quad K_x=K_{\rm iso}+\delta, \quad K_y=K_{\rm iso}-\frac{\delta}{2}(1+\eta),$$

$$K_z=K_{\rm iso}-\frac{\delta}{2}(1-\eta),$$

$$\text{(case 3)} \quad K_x=K_{\rm iso}-\frac{\delta}{2}(1-\eta), \quad K_y=K_{\rm iso}+\delta,$$

$$K_z=K_{\rm iso}-\frac{\delta}{2}(1+\eta). \tag{15}$$

After performing the averages over ϕ, θ, and φ, the results for the $|C|^2$ and α are shown for each case in Appendix B.

Finally, taking into account that $\mathbf{H}=(0,0,H_0)$ in the laboratory frame, the $T_1^{-1}(\gamma)$ is given by the following formula:

$$T_1^{-1}(\gamma)=\tfrac{1}{5}\sum_{\substack{j=0,2\\k=\mathrm{Re,Im}}}(F_j^L)^2 2\{|C_{k,j,2}|^2\tilde{\mathcal{I}}(4E_{\mathrm{rot}}) + |C_{k,j,1}|^2\tilde{\mathcal{I}}(E_{\mathrm{rot}})\}\{\alpha_k(j,1)\}^2H_0^2, \quad (16)$$

where

$$\tilde{\mathcal{I}}(\lambda E_{\mathrm{rot}})=\frac{1/\lambda E_{\mathrm{rot}}}{1+(\omega_0/\lambda E_{\mathrm{rot}})^2}. \quad (17)$$

IV. RESULTS OF THE CALCULATIONS

A. ^{13}C NMR spectra in the presence of the uniaxial rotation motion

In Fig. 10 we show the calculated line shape (dotted line) assuming that the NMR shift tensor is axial ($\eta=0$) with the symmetry axis along z, that is, normal to the sphere. The circulation of the three principal values in the shift tensor does not produce any difference in the results. We choose here the shift tensor (290, 290, -70), which is appropriate for reproducing the observed spectrum of Rb_3C_{60}. The line shape shows a characteristic form, with a sharp line at the position of K_{iso}, a shoulder and a broad tail. A small discrepancy around the central peak may be due to an inhomogeneity of the τ_c for the perpendicular motion.

In Fig. 11 we display that obtained for $\eta=1$ (dotted line), which was assumed in our previous paper for K_3C_{60}.[9] The principal values of the shift tensor are taken to be (32, 340, 186), where the last value corresponds to K_z, normal to the sphere. Here again, the sharp peak originating from the K_{iso} and the broad tail are found.

Also demonstrated in Figs. 10 and 11 is the comparison of the calculated line shape with the observed spectra (solid line) for the ^{13}C NMR of Rb_3C_{60} at 365 K and of K_3C_{60} at 255 K, respectively. The agreement between them is satisfactory. This fact suggests that the uniaxial motion is well established in the two compounds at those temperatures.

On the other hand, as mentioned early in connection with the disappearance of the tail, the spin-echo spectrum at the same temperature does not coincide with the calculated line shape (Figs. 2, 11 and Figs. 7, 10). This is however due to the fact that the slow motion of the C_{60} also takes place in the real system. We will come back to this point later in the discussion of T_2^{-1}.

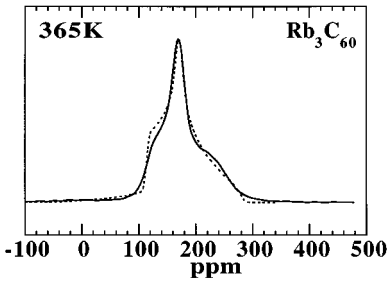

FIG. 10. Fourier transformed spectra of ^{13}C FID signals (solid line) measured at 365 K in Rb_3C_{60} and calculated result (dotted line) [for the uniaxial rotational jump motion. The shift tensor (290, 290, -70) is used in this calculation].

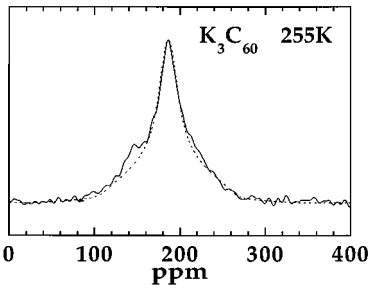

FIG. 11. Fourier transform spectra of the ^{13}C FID signals (solid line) measured at 255 K in K_3C_{60} and calculated result (dotted line) [for the uniaxial rotational jump motion. The shift tensor (32, 340, 186) is used in this calculation].

It seems worthwhile to determine whether we can associate the actual features in the spectra to specific rotation angles γ with respect to the applied field. Figures 12 and 13 show the θ dependence of the line shapes for the cases of the shift tensors used above. Angles indicated in the figures represent a range of γ values. (Since the line shapes shown in Figs. 12 and 13 are obtained by summing up all contributions for the various γ ranges indicated, the amplitude of each line shape correctly reflects the relative intensities.) As seen in the figures, the line shape at 50°–60° is always narrow as compared with the others. This is due to the rotation close to the magic angle. On the other hand, it is found that the broad tail originates from the C_{60} with rotation axes close to and far from the direction of the external field.

B. Dynamical character in the presence of the uniaxial motion

1. Spin-spin relaxation time T_2^{-1}

Figure 14 represents the time averaged shift (σ_{ZZ}) as a function of θ for the γ values indicated in the figure, where only the $\eta=0$ symmetry is considered for simplicity (the results for $\eta=1$ is essentially identical). This figure is nothing else but a visualization of Eq. (3). The figure shows the different values of the average shift at each carbon site. It is quite clear that the average shift for a given carbon atom will

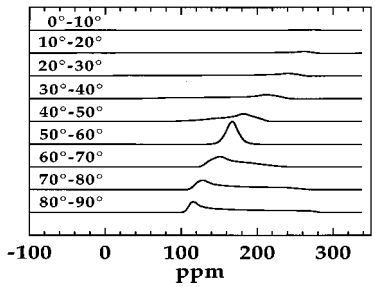

FIG. 12. Dependence of the calculated line shapes with the orientation of the rotation axis with respect to the external field. The spectra are calculated for the shift tensor (290, 290, -70) for the range of γ values indicated in the figure.

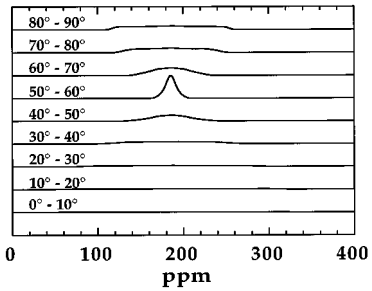

FIG. 13. Dependence of the calculated line shapes with the orientation of the rotation axis with respect to the external field. The spectra are calculated for the shift tensor (32, 340, 186) for the range of γ values indicated in the figure.

change each time when a perpendicular flip of the C_{60} occasionally happens. Since the T_2^{-1} is sensitive to fluctuating components of the local field along the external field ($=\sigma_{ZZ}H_0$), it is obvious that the slowing down of this perpendicular motion is the origin of the short T_2 component which appears around 300 K in our previous ^{13}C-NMR experiment. The rapid increase of T_2^{-1} is simply due to a large activation energy for this flipping motion. The intensity loss in the tail of the spin-echo FT spectrum can also be certainly explained by the fact that the C_{60} molecules rotating around an axis far from the magic angle, which contribute to the tail, are sensing the largest fluctuations of σ_{ZZ} when the flipping occurs, which gives rise to the short T_2^{-1}.

On the other hand, the carbons on the C_{60} molecules which rotate at γ close to the magic angle see little variation in the averaged shift, as long as the fast rotation always takes place around the same rotation axis. As pointed out in Sec. III, this condition should result in a δ-function-like peak at $K_{\rm iso}$ in the spectrum. If the fast rotation axis did also change in time, we would even lose the spin-echo signal for moderately long spin echo delays because all the carbons would be forced to see different averaged fields from time to time.

Then what is the dominant T_2 relaxation process for the sharp peak corresponding to crystallites in which the C_{60} are rotating at magic angle spinning? Here, we should remind that the natural abundance of ^{13}C, 1.1%, corresponds statistically to less than one ^{13}C per C_{60} molecule. Therefore the nuclear spin dipole-dipole interaction is negligible inside a given C_{60}. Even if two ^{13}C exist in a same ball, their dipole-dipole interaction is averaged by magic angle spinning.

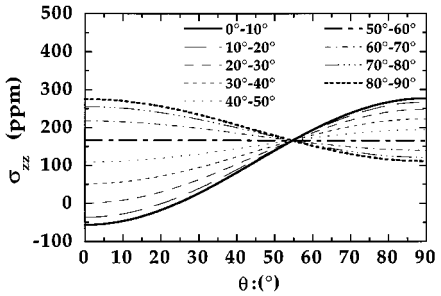

FIG. 14. Time averaged shift (σ_{ZZ}) along the external field with η=0 as a function of the position θ of the C atom on the sphere for the γ values of the rotation axis indicated in the figure.

Therefore, only the source for T_2 certainly arises from the dipole interaction between ^{13}C in different C_{60}'s and ^{13}C and cation ions, because the rotational motion of the balls do not correspond to a common magic angle rotation for the two ^{13}C spins. In this case, we can expect that the sharp peak should decay with a T_2 at its static limit, which could be estimated from a second moment calculation in which we assumed a point model for the C_{60} balls (in a point lattice the abundance of ^{13}C at the C_{60} site is replaced by $60\times1.1\%$).

This is quite consistent with our observation that a small contribution in T_2^{-1} was always observed in the whole investigated T range, with an absolute value in excellent agreement with that derived through the above second moment calculation.[9] Therefore, the rotation at the magic angle must be responsible for the observation of the sharp peak in the spectrum from the echo signal (Figs. 2 and 7). These arguments are enough to allow us to conclude that the fast rotation axis does not change to other possible axes at least during the time scale of T_2. The fact that the orientational axes are well established in the lattice implies that the symmetry of the crystal field at the C_{60} site is lower than cubic.

There seems to exist inconsistency in understanding the molecular motion in pristine C_{60} in the high temperature phase between NMR (Refs. 4 and 6) and x-ray experiments,[7] where the former result has been understood by an isotropic diffusive motion while the latter claims that the motion is anosotropic. The ^{13}C-NMR spectra taken from FID and spin echo would provide critical information to understand the molecular dynamics in pristine C_{60}.

2. Spin-lattice relaxation rate T_1^{-1}

Here, it is quite worthwhile to check whether the recovery curve for T_1 can also be explained consistently within the framework used here, namely whether it shows a single exponential behavior or it implies a multiexponential curvature.

The recovery curve is easily described by the following equation with the use of the $T_1(\gamma)$ derived in Sec. III:

$$\frac{M_0-M(t)}{M_0}\propto\sum_{\gamma}\exp\left(\frac{-t}{T_1(\gamma)}\right)\sin\gamma. \tag{18}$$

That is, the curve is reproduced by a sum of all magnetizations decaying at the γ-dependent T_1 at the given time. The $\sin\gamma$ in the right side originates from the distribution of the rotation axis with respect to the external field. As seen in Fig. 15 [where (340, 32, 186) is used for the shift tensor for K_3C_{60}], all the curves surprisingly show a single exponential recovery in spite of the γ dependence in the $|C|^2$ given in Appendix B. Other combinations of the shift values also result in the single exponential behavior. Therefore, our model of the uniaxial rotation motion around a fixed axis with occasional perpendicular flips can reproduce properly the experimental observation that the recovery curves could be nicely fitted to $\exp(-t/T_1)$ with a unique T_1 in the T range where the uniaxial motion takes place.[9] The estimated values from the recovery curves give $\sim$0.73 sec for case 2 and case 3, and $\sim$0.5 sec for case 1, none of which meets perfectly the measured contribution of the rotational motion $T_1\sim1.25\pm0.25$ sec.[9] Since the shift tensor values are assumed to be independent of the carbon site in this analysis, this small discrepancy may suggest that the charge distribu-

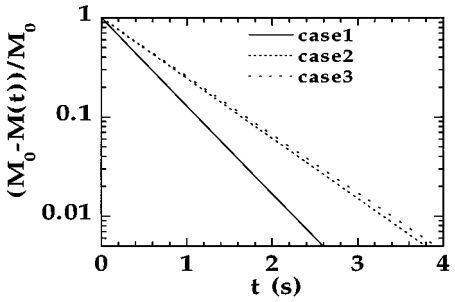

FIG. 15. Recovery curve calculated with Eq. (18). The solid, dotted, and broken lines are the calculated recovery curves corresponding to case 1, case 2, and case 3, respectively, as defined in Eq. (15).

tion on the carbon sites is not uniformly spread, as has been claimed from x-ray diffraction analysis.[21,22] The T_1 might then be more sensitive to the on-site charge than the features appearing in the static spectra.

The observed nonsingle exponential recovery curve below about 160 K (Ref. 9) can be naturally explained by the slowing down of the perpendicular motion, as the correlation time expected from τ_c^s in Fig. 1 becomes comparable to T_1 around 160 K. This situation can no longer average out the distribution of T_1 associated with the γ dependence.

C. Spectra in the frozen state

Figures 16 and 17 are the line shapes calculated for the $\eta=0$ and 1 symmetries in the frozen state (dotted line). In contrast to the ones in the presence of the uniaxial motion, the calculated line shapes are regular three-dimensional powder patterns in a uniformly distributed system. In principle, the symmetry and the values of the shift tensor should be determined from the frozen state spectrum at very low T by comparison with the calculated line shape. However, the line shapes observed in K_3C_{60} and Rb_3C_{60} just above their superconducting transition temperature cannot be explained from the shift tensor values deduced from the fits to the spectra above the respective T^* with the uniaxial rotation motion.

Here, we should remind that a phase transition occurs at 200 K in K_3C_{60} and possibly around 380 K in Rb_3C_{60}. Its occurrence as well as the freezing of the motion could modify the electronic state on the C_{60} molecule and cause further modifications of the crystal field. The existence of

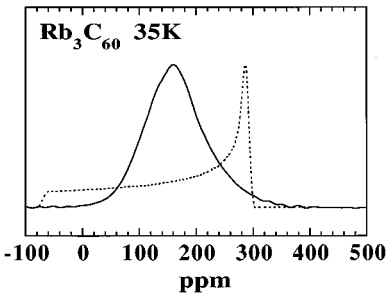

FIG. 16. Fourier transformed spectra of the ^{13}C FID signals (solid line) measured at 35 K in Rb_3C_{60} and calculated result (dotted line). (290, 290, −70) is used for the calculated line shape.

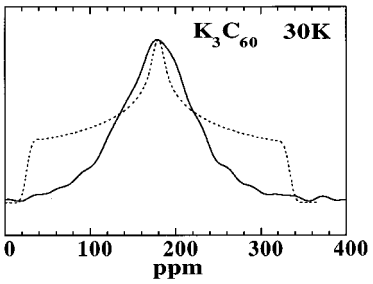

FIG. 17. Fourier transform spectra of the ^{13}C FID signals (solid line) measured at 30 K in K_3C_{60} and calculated static spectrum (dotted line) with (32, 340, 186) obtained from the best fit in Fig. 11.

three distinct carbon sites in the frozen state will also produce an inhomogeneity of the charge distribution on the carbon sites. A synchrotron x-ray experiment performed on the pristine C_{60} compound at 300 K claimed the existence of a nonuniform distribution of charge density on the C_{60} surface.[21] The deduced charge distribution shows density deficiency of 16% in ⟨1,1,1⟩ directions and 10% excess about ⟨1,1,0⟩, even though the C_{60} molecule at that temperature makes a rapid reorientational motion. The same experiment on Li_2CsC_{60} has however shown that the excess density is along the ⟨1,1,1⟩ axis towards the Li ions.[22] The existence of the alkali ions seems already enough to modify the electronic charge distribution on the C_{60} molecule. These multiple effect would produce even more than three nonequivalent carbon sites at low T.

V. DISCUSSION

We demonstrated so far that the NMR results can be satisfactorily explained by the presence of the uniaxial motion. On the contrary, the observed line shapes at low temperature are not well understood. Although the discrepancy could be attributed to the occurrence of the phase transition, its nature and relationship to the appearance of the third line in the K and Rb spectra below T^* are not clear. Walstedt *et al.* have performed NMR double resonance[14] on ^{87}Rb in Rb_3C_{60} and assigned the third Rb line to T sites slightly offset from the ideal position (T'). On the other hand, Apostol *et al.*[23] claimed that this extra peak comes from the T sites in the vicinity of an empty T site. In this interpretation, the T ions perform in high temperature an internal jump between vacancies existing at the T sites, while the motion is frozen gradually as temperature lowers. They claimed that when the jumping rate becomes comparable to the NMR time scale, then the third line is detected. The vacancy concentration is estimated to be 1.3%. Since the existence of such a vacancy breaks the local charge neutrality, the absence of a positive charge at the T site should produce a large distortion of an electric potential at the surrounding sites. This situation would give rise to a large quadrupole interaction for the cation nuclear spins sitting at both T and O sites near the empty site (the quadrupole interaction couples the nuclear spins to the electric field gradient). Although the estimated concentration is very small, since the Coulomb interaction is effective over long distance the line shape of the regular T and O sites should be modified through the quadrupole interaction,

which does not seem to be the case.[18] Let us point out that large quadrupolar effects have been seen in the polymer phase of RbC_{60} which has an orthorombic symmetry but for which the charge neutrality is ensured locally.[24] It is then somewhat difficult to accept this interpretation for the appearance of T' peak, although more refined analyses of the data are necessary to ensure this point and are presently undertaken. Walsteds *et al.* have ruled out this possibility by claiming that the thermally activated internal jumps should also take place between T and O sites.[14]

Recently, Pintschovius *et al.* have performed diffuse x-ray and neutron scattering experiment on single crystal of pristine C_{60} and found a pronounced orientational order with a coherence length of about 40 Å at 265 K, which is above its disordered-ordered phase transition temperature.[25] This result clearly indicates that a precursor for the orientational ordering already sets in above its phase transition temperature. Although it is not yet clarified whether the perpendicular motion exists in pristine C_{60}, the situation of the high temperature phase looks very similar to that observed in the high T phase in K_3C_{60}. From this point of view, we may argue that the phase transition in K_3C_{60} might as well correspond to an ordering of the rotation axis. As mentioned in Sec. II A 2, the broadening of the ^{39}K lines above T^* can be assigned to the slowing down of the perpendicular motion. The discontinuous change of the broadening rate across T^* suggests some connection between the phase transition and the freezing of this motion. Although we claimed from the analysis of the ^{13}C spectra that the rotation axes are well fixed in the lattice within a time scale of 10^{-4} sec, it is not clear whether they are randomly distributed with respect to the lattice. The phase transition might correspond to an increase of the correlation length of the orientation of the rotation axes. This increased orientational order could create a distinction between cation sites. Recently, Zimmer *et al.* discussed the appearance of the T' peak in terms of a disordering associated with the thermally activated occupation of the different C_{60} orientation rather than the chemical exchange. The evolution of the observed Rb spectra appeared to be reasonably reproduced with activation energy 580 meV and 15% probability for the T' site.[26]

However, there is no experimental report so far suggesting the change of the lattice parameter in K_3C_{60} around 200 K, while it has been well known in pure C_{60}. More refined structural and NMR data are required to understand how far one can discuss the phase transition in connection with the appearance of T' peak along with taking the analogy found in both systems.

VI. SUMMARY

We presented here some experimental results on ^{13}C and alkali NMR in the M_3C_{60} compounds. We have performed numerical calculations of the ^{13}C line shapes, assuming the uniaxial rotational motion of the C_{60} with occasional flips perpendicular to the fixed rotation axis. The agreements between the calculated and observed line shapes strongly support the presence of this characteristic molecular motion on the C_{60} in M_3C_{60} and conclude that the rotation axis is well established in the lattice. The existence of such preferential axis for the uniaxial motion implies that the crystal field at the C_{60} site is distorted and has a lower symmetry than cubic. We have stressed that the uniaxial motion persists through the phase transition.

On the other hand, the line shape at low T could not be reproduced using the shift tensor deduced above T^*. The appearance of the T' line in the alkali NMR spectra below T^*, which suggests the occurrence of some modification in the crystal structure accompanied with the freezing of the molecular motions. The existence of at least three kinds of carbons in the frozen state seem to modify significantly the electronic state on the C_{60} balls.

APPENDIX A

The $C_{k,m,j}(\Omega)$ and $\alpha_k(m,j)$, where the orientation of the system can be described in polar coordinates, are given as follows:

$$
\begin{aligned}
&C_{\mathrm{Re}\,0,0}=\tfrac{1}{2}(3\cos^2\theta-1), && \alpha_{\mathrm{Re}}(0,0)=1, && C_{\mathrm{Re}\,2,0}=\frac{\sqrt{6}}{2}(\cos^2\varphi-\sin^2\varphi)\sin^2\theta, && \alpha_{\mathrm{Re}}(2,0)=1,\\
&C_{\mathrm{Re}\,0,1}=\sqrt{\frac{3}{8}}\sin 2\theta, && \alpha_{\mathrm{Re}}(0,1)=\sqrt{6}, && C_{\mathrm{Re}\,2,1}=\frac{\sqrt{3}}{2}(\sin^2\varphi-\cos^2\varphi)\sin 2\theta, && \alpha_{\mathrm{Re}}(2,1)=\sqrt{2},\\
&C_{\mathrm{Re}\,0,2}=\sqrt{\frac{3}{8}}\sin^2\theta, && \alpha_{\mathrm{Re}}(0,2)=2\sqrt{6}, && C_{\mathrm{Re}\,2,2}=\frac{1}{\sqrt{10}}(\cos^2\varphi-\sin^2\varphi)(\cos^2\theta+1), && \alpha_{\mathrm{Re}}(2,2)=2\sqrt{15},\\
&C_{\mathrm{Im}\,0,0}=0, && \alpha_{\mathrm{Im}}(0,0)=0, && C_{\mathrm{Im}\,2,0}=0, && \alpha_{\mathrm{Im}}(2,0)=0,\\
&C_{\mathrm{Im}\,0,1}=0, && \alpha_{\mathrm{Im}}(0,1)=0, && C_{\mathrm{Im}\,2,1}=\sqrt{\frac{3}{5}}\sin 2\varphi\,\sin\theta, && \alpha_{\mathrm{Im}}(2,1)=\sqrt{10},\\
&C_{\mathrm{Im}\,0,2}=0, && \alpha_{\mathrm{Im}}(0,2)=0, && C_{\mathrm{Im}\,2,2}=-\sqrt{\frac{6}{5}}\sin 2\varphi\cos\theta, && \alpha_{\mathrm{Im}}(2,2)=2\sqrt{5}. \qquad \text{(A1)}
\end{aligned}
$$

If the motion is random and isotropic, $E_{\mathrm{rot}}=E_{\mathrm{flip}}=E\equiv 1/6\tau_c$ and all products of the $|C|^2$ in Eq. (13) are equal to 1/5. After applying commutation rules to the spin operators and paying attention to the fact that $\mathbf{H}=(0,\,0,\,H_0)$ in the laboratory frame, we find back the ordinary expression,[19]

$$T_1^{-1}=\frac{6}{40}\,(\gamma\delta H_z)^2\left(1+\frac{\eta^2}{3}\right)\frac{2\tau_c}{1+(\omega_0\tau_c)^2}. \tag{A2}$$

APPENDIX B

Case 1:

$$\begin{aligned}
|C_{\mathrm{Re}\,0,2}|^2&=\tfrac{8}{695}(25-22\cos^2\gamma+9\cos^4\gamma), & \alpha_{\mathrm{Re}}(0,2)&=\frac{3\sqrt{695}}{16\sqrt{2}},\\
|C_{\mathrm{Re}\,0,1}|^2&=\tfrac{8}{205}(4+9\cos^2\gamma-9\cos^4\gamma), & \alpha_{\mathrm{Re}}(0,1)&=\frac{3\sqrt{205}}{16\sqrt{2}},\\
|C_{\mathrm{Re}\,2,2}|^2&=\tfrac{8}{4535}(89+42\cos^2\gamma+9\cos^4\gamma), & \alpha_{\mathrm{Re}}(2,2)&=\frac{\sqrt{4535\times 6}}{32},\\
|C_{\mathrm{Re}\,2,1}|^2&=\tfrac{8}{845}(20+29\cos^2\gamma-29\cos^4\gamma), & \alpha_{\mathrm{Re}}(2,1)&=\frac{13\sqrt{30}}{32},\\
|C_{\mathrm{Im}\,0,2}|^2&=\tfrac{2}{35}(3+\sin^2\gamma), & \alpha_{\mathrm{Im}}(0,2)&=\frac{3\sqrt{35}}{4\sqrt{2}},\\
|C_{\mathrm{Im}\,0,1}|^2&=\tfrac{2}{35}(3+\cos^2\gamma), & \alpha_{\mathrm{Im}}(0,1)&=\frac{3\sqrt{35}}{8\sqrt{2}},\\
|C_{\mathrm{Im}\,2,2}|^2&=\tfrac{2}{55}(4+3\cos^2\gamma), & \alpha_{\mathrm{Im}}(2,2)&=\frac{5\sqrt{66}}{8},\\
|C_{\mathrm{Im}\,2,1}|^2&=\tfrac{2}{55}(4+3\sin^2\gamma), & \alpha_{\mathrm{Im}}(2,1)&=\frac{5\sqrt{66}}{16}.
\end{aligned} \tag{B1}$$

Case 2:

$$\begin{aligned}
|C_{\mathrm{Re}\,0,2}|^2&=\tfrac{8}{5925}(143-6\cos^2\gamma+27\cos^4\gamma), & \alpha_{\mathrm{Re}}(0,2)&=\frac{15\sqrt{237}}{64},\\
|C_{\mathrm{Re}\,0,1}|^2&=\tfrac{8}{1255}(28+27\cos^2\gamma-27\cos^4\gamma), & \alpha_{\mathrm{Re}}(0,1)&=\frac{3\sqrt{1255}}{64},\\
|C_{\mathrm{Re}\,2,2}|^2&=\tfrac{8}{17045}(539-354\cos^2\gamma+171\cos^4\gamma), & \alpha_{\mathrm{Re}}(2,2)&=\frac{\sqrt{177045\times 6}}{64},\\
|C_{\mathrm{Re}\,2,1}|^2&=\tfrac{8}{4535}(92+171\cos^2\gamma-171\cos^4\gamma), & \alpha_{\mathrm{Re}}(2,1)&=\frac{\sqrt{907\times 30}}{64},\\
|C_{\mathrm{Im}\,0,2}|^2&=\tfrac{2}{345}(28+13\cos^2\gamma), & \alpha_{\mathrm{Im}}(0,2)&=\frac{3\sqrt{345}}{16},\\
|C_{\mathrm{Im}\,0,1}|^2&=\tfrac{2}{345}(28+13\sin^2\gamma), & \alpha_{\mathrm{Im}}(0,1)&=\frac{3\sqrt{345}}{32},\\
|C_{\mathrm{Im}\,2,2}|^2&=\tfrac{2}{905}(89+3\sin^2\gamma), & \alpha_{\mathrm{Im}}(2,2)&=\frac{\sqrt{5430}}{16},\\
|C_{\mathrm{Im}\,2,1}|^2&=\tfrac{2}{905}(89+3\cos^2\gamma), & \alpha_{\mathrm{Im}}(2,1)&=\frac{\sqrt{5430}}{32}.
\end{aligned} \tag{B2}$$

Case 3:

$$
\begin{aligned}
|C_{\mathrm{Re}\,0,2}|^2 &= \tfrac{8}{5925}(143-6\cos^2\gamma+27\cos^4\gamma), & \alpha_{\mathrm{Re}}(0,2) &= \frac{15\sqrt{237}}{64},\\
|C_{\mathrm{Re}\,0,1}|^2 &= \tfrac{8}{1255}(28+27\cos^2\gamma-27\cos^4\gamma), & \alpha_{\mathrm{Re}}(0,1) &= \frac{3\sqrt{1255}}{64},\\
|C_{\mathrm{Re}\,2,2}|^2 &= \tfrac{8}{17045}(539-354\cos^2\gamma+171\cos^4\gamma), & \alpha_{\mathrm{Re}}(2,2) &= \frac{\sqrt{17045\times 6}}{64},\\
|C_{\mathrm{Re}\,2,1}|^2 &= \tfrac{8}{4535}(92+171\cos^2\gamma-171\cos^4\gamma), & \alpha_{\mathrm{Re}}(2,1) &= \frac{\sqrt{4535\times 6}}{64},\\
|C_{\mathrm{Im}\,0,2}|^2 &= \tfrac{2}{345}(28+13\cos^2\gamma), & \alpha_{\mathrm{Im}}(0,2) &= \frac{3\sqrt{345}}{16},\\
|C_{\mathrm{Im}\,0,1}|^2 &= \tfrac{2}{345}(28+13\sin^2\gamma), & \alpha_{\mathrm{Im}}(0,1) &= \frac{3\sqrt{345}}{32},\\
|C_{\mathrm{Im}\,2,2}|^2 &= \tfrac{2}{665}(41+51\sin^2\gamma), & \alpha_{\mathrm{Im}}(2,2) &= \frac{\sqrt{665\times 6}}{16},\\
|C_{\mathrm{Im}\,2,1}|^2 &\tfrac{2}{665}(41+51\cos^2\gamma), & \alpha_{\mathrm{Im}}(2,1) &= \frac{\sqrt{665\times 6}}{32}.
\end{aligned}
\tag{B3}
$$

*Present address: Los Alamos National Laboratory, Los Alamos, NM 87545.

†Permanent address: Research Institute for Solid State Physics, P.O.B. 49, H-1525 Budapest, Hungary.

‡Present address: Department of Physics and Chemistry and Biochemistry, University of California, Los Angeles, CA 90024-1569.

[1] H. W. Kroto, J. R. Heath, S. C. O'Brien, R. F. Curl, and R. E. Smalley, Nature **318**, 162 (1986).

[2] A. F. Hebard, M. J. Rosseinsky, R. C. Haddon, D. W. Murphy, S. H. Glarum, T. T. M. Palstra, A. P. Ramirez, and A. R. Kortan, Nature **350**, 600 (1991).

[3] K. Holczer, O. Klein, S.-M. Huang, R. B. Kaner, K.-J. Fu, R. L. Whetten, and F. Diederich, Science **252**, 1154 (1991).

[4] R. Tycko, G. Dabbagh, R. M. Fleming, R. C. Haddon, A. V. Makhija, and S. M. Zahurak, Phys. Rev. Lett. **67**, 1886 (1991).

[5] Y. Maniwa, K. Mizoguchi, K. Kume, K. Kikuchi, I. Ikemoto, S. Suzuki, and Y. Achiba, Solid State Commun. **80**, 609 (1991).

[6] R. D. Johnson, C. S. Yannoni, H. C. Dorn, J. R. Salem, and D. S. Bethune, Science **225**, 1235 (1992).

[7] P. A. Heiney, J. E. Fischer, A. R. McGhie, W. J. Romanow, A. M. Denenstein, J. P. McCauley, Jr., A. B. Smith III, and D. E. Cox, Phys. Rev. Lett. **66**, 2911 (1991).

[8] R. Moret, P. A. Albouy, V. Agafonov, R. Ceolin, D. André, A. Dworkin, H. Szwarc, C. Fabre, A. Rassat, A. Zahab, and P. Bernier, J. Phys. (France) I **2**, 511 (1992).

[9] Y. Yoshinari, H. Alloul, G. Kriza, and K. Holczer, Phys. Rev. Lett. **71**, 2413 (1993).

[10] G. Zimmer, M. Helme, M. Mehring, and F. Rachdi, Europhys. Lett. **27**, 543 (1994).

[11] P. W. Stephens, L. Mihaly, P. L. Lee, R. L. Whetten, S. M. Huang, R. Kaner, F. Deiderich, and K. Holczer, Nature **351**, 632 (1991).

[12] W. I. F. David, R. M. Ibberson, T. J. S. Dennis, J. P. Hare, and K. Prassides, Europhys. Lett. **18**, 219 (1992).

[13] R. Blinc, J. Seliger, J. Dolinsek, and D. Arcon, Phys. Rev. B **49**, 4993 (1994).

[14] R. E. Walstedt, D. W. Murphy, and M. Rosseinsky, Nature **362**, 661 (1993).

[15] S. E. Barretand R. Tycko, Phys. Rev. Lett. **69**, 3754 (1992).

[16] H. Alloul, K. Holczer, Y. Yoshinari, and O. Klein, Physica C **235-240**, 2509 (1994).

[17] R. Tycko, G. Dabbagh, M. J. Rosseinsky, D. W. Murphy, A. P. Ramirez, and R. M. Fleming, Phys. Rev. Lett. **68**, 1912 (1992).

[18] Y. Yoshinari, H. Alloul, K. Holczer, and L. Forro, Physica C **235-240**, 2479 (1994).

[19] A. Abragam, *Principles of Nuclear Magnetism* (Oxford University, New York, 1961); C. P. Slichetr, *Principle of Nuclear Magnetic Resonance*, 3rd ed. (Springer-Verlag, Berlin, 1992).

[20] W. T. Huntress, Jr., Phys. Rev. B **48**, 3524 (1968).

[21] P. C. Chow, X. Jiang, G. Reiter, P. Wochner, S. C. Moss, J. D. Axe, J. C. Hanson, P. K. McMullan, R. L. Meng, and C. W. Chu, Phys. Rev. Lett. **69**, 2943 (1992).

[22] I. Hirosawa, K. Prassides, J. Mizuki, K. Tanigaki, M. Gevaert, A. Lappas, and J. K. Cockcroft, Science **264**, 1294 (1994).

[23] M. Apostol, C. Goze, F. Rachdi, M. Mehring, and J. E. Fischer, Solid State Commun. **98**, 253 (1996).

[24] V. Brouet, Y. Yoshinari, H. Alloul, and L. Forro, Physica C **235-240**, 2481 (1994).

[25] L. Pintschovius, S. L. Chaplot, G. Roth, and G. Heger, Phys. Rev. Lett. **75**, 2843 (1995).

[26] G. Zimmer, K.-F Thier, M. Mehring, F. Rachdi, and J. E. Fischer, Phys. Rev. B **53**, 5620 (1996).